Title:

Sway-rocking spring system applicable to short-rigid monopile foundations

Authors:

Yukiho Kamata [a] and Akihiro Takahashi [b*]

[a] Kajima Corporation, Tokyo, Japan

(Formerly Department of Civil and Environmental Engineering, Tokyo Institute of Technology, Tokyo, Japan)

Email: kamatay@kajima.com

[b] Department of Civil and Environmental Engineering,

Tokyo Institute of Technology

2-12-1-M1-3 Oh-okayama, Meguro, Tokyo 152-8552, Japan

Tel: +81-(0)3-5734-2593 Fax: +81-(0)3-5734-3577

Email: takahashi.a.al@m.titech.ac.jp

*Corresponding author

Geotechnical and Geological Engineering, 39(4), 3065-3079, 2021

Original URL:

https://doi.org/10.1007/s10706-021-01678-2

Abstract

Sway-Rocking (SR) spring system is a foundation modelling method in which a 2×2 spring stiffness matrix represents the foundation stiffness at seabed level. Since each individual element of the spring stiffness matrix is a function of a few physical properties of the soil and pile, it is the simplest and computationally cheapest method to estimate the deformation at the seabed level and the natural frequency of an offshore wind turbine structure. Formulae currently available are only applicable to conventional long-flexible piles or perfectly rigid foundations such as footings or caissons. This study aims to extend the application of the SR spring system to a so-called short-rigid pile range, which lays between the two ranges: long-flexible and perfectly rigid. Monopiles, the most commonly selected type of offshore wind foundations, are categorized in the short-rigid pile range. By conducting three-dimensional finite element analyses, the short-rigid pile behaviour is investigated. Based on the results, a new set of formulae of the SR spring stiffness, which is applicable to a wide range (long-flexible, short-rigid and perfectly rigid) of piles, is proposed. The new formulae also improve the accuracy of frequency estimation for practical use cases.

Keywords

offshore wind turbine structure; monopile; short-rigid pile; Sway-Rocking spring system; natural frequency

1. Introduction

In the last decade, the offshore wind industry has vastly developed to become one of the largest renewable energy sectors. Especially in the last years, commercial offshore wind farms are under development not only in Europe but also in America and Asia. Along with the acceleration of worldwide development of the offshore wind farms, the size of wind turbine generators (WTG) is exponentially increasing as pictured in **Fig. 1** (Data source: Wind-Europe 2017; 4C Offshore 2018; and IRENA 2019). It is expected that the 12 MW size turbines will become the world standard in the upcoming 5 years.

The most commonly used supporting structure type till now is the pile foundation due to its relatively low construction cost and ease of installation in shallow to intermediate water depths. This type of foundation is composed of a monopile, which is installed into the seabed, and a transition piece, which connects a WTG tower and the monopile. Along with the development of WTG generators with larger energy yielding capacities, the diameter of monopiles has increased up to 10 m. As a result, the slenderness ratio (L_p/D_p) of state-of-the-art monopiles decreases to less than 10 while most conventional friction piles have a slenderness ratio of more than 20. Hence, these monopiles are no longer considered as long-flexible foundations but as short-rigid structures closer to caissons. Short-rigid structures show different behaviour than conventional long-flexible piles. If the size effect of rigid piles with lower slenderness ratio (L_p/D_p) such as base shear and moment and a distributed moment along the pile is taken into account as studied in the PISA project (Byrne 2020), a more economical and optimized design will be possible. Hence, the short-rigid pile behaviour should be further studied and novel design methods should be developed.

Monopiles are exposed to cyclic lateral loads due to the rotating blades and environmental loads such as wind and waves. According to Arany et al. (2016), the natural frequency of WTG

structures is designed to be between the rotor frequency (1P) and blade passing frequency (3P). To accurately estimate the natural frequency, the foundation stiffness should be considered. Finite element analyses and frame calculations with Winkler springs along the pile is recommended by DNVGL-RP-C212 (2017) and often-used by WTG foundation designers. However, these methods are computationally more expensive. For Service Limit State (SLS), the pile deflection at seabed level and the natural frequency of a tower-foundation system should be assessed. A simpler method, which is called the Sway-Rocking (SR) spring system, is available as introduced by Bhattacharya (2019).

The SR spring system is a foundation modelling method where the soil-pile interaction is modelled with a lateral spring (K_L), a rotational spring (K_R) and coupling springs (K_{LR} and K_{RL}) at the seabed as shown in **Fig. 2**. Since the vertical spring K_V is an independent element which does not interact with the SR spring system, discussion on the vertical spring is avoided in this paper. For estimation of K_V value, see Fleming et al. (1992) and DNV (2002). The spring stiffness can be used to estimate lateral deformation: *u* and the rotation: ϑ at the seabed level from the excitation horizontal loading: *H* and the moment: *M* and vice versa as shown in **Eqn. (1)**.

$$\begin{bmatrix} H \\ M \end{bmatrix} = \begin{bmatrix} K_L & K_{LR} \\ K_{RL} & K_R \end{bmatrix} \begin{bmatrix} u \\ \theta \end{bmatrix} \qquad (1)$$

Using this method, the soil-pile interaction can be easily elaborated in the natural frequency estimation and the dynamic analysis of the WTG structure during the preliminary design phase.

The SR spring stiffness for long-flexible piles is determined by the soil stiffness (E_s), pile diameter (D_p) and soil-pile stiffness ratio (E_s/E_p) but not the slenderness ratio (L_p/D_p) because the conventional piles are longer than a critical pile length, that means these piles would have the same behaviour as infinitely long piles. Randolph (1981) proposed stiffness

92 formulae for long-flexible piles embedded in a linear elastic homogeneous soil. Several
93 researchers have proposed modified formulae for not only homogeneous soils, which aims at
94 over-consolidated clay, but also parabolic inhomogeneous (sandy soil) and linear
95 inhomogeneous (normally consolidated clay) according to Shadlou et al. (2016). The ones
96 proposed by Gazetas (1984) are recommended in Eurocode 8 (2004). According to the
97 references Randolph (1981) and Gazetas (1984), the non-dimensional spring stiffness η, which
98 is defined in **Eqns. (2) ~ (5)**, is a power function of the stiffness ratio (pile effective stiffness /
99 soil stiffness).

100 $$\eta_L = K_L/E_s D_p \qquad (2)$$

101 $$\eta_{LR} = K_{LR}/E_s {D_p}^2 \qquad (3)$$

102 $$\eta_{RL} = K_{RL}/E_s {D_p}^2 \qquad (4)$$

103 $$\eta_R = K_R/E_s {D_p}^3 \qquad (5)$$

104 On the other hand, as for perfectly rigid piles such as footing or caisson type of foundations,
105 the mechanical behaviour is influenced by the soil stiffness (E_s), pile diameter (D_p) and
106 slenderness ratio (L_p/D_p) but not the stiffness ratio (E_s/E_p), as the deflection is negligibly
107 small. Carter et al. (1992) proposed stiffness formulae for shaft foundations in linear elastic
108 homogeneous grounds as a power function of the slenderness ratio (L_p/D_p), that became the
109 foundation of perfectly rigid pile modelling with the SR spring system. Higgins et al. (2013)
110 have recently extended the SR modelling method to perfectly rigid pile foundations in soil with
111 stiffness proportional to depth as well as in double-layered soil with two different
112 homogeneous profiles.

113 State-of-the-art monopiles are categorized between conventional long-flexible piles and
114 perfectly rigid piles and exhibit characteristics of the both. In this study, these types of piles
115 are named as short-rigid. The SR spring stiffness of the short-rigid type of piles will be defined

as a function of both stiffness ratio (E_s/E_p) and slenderness ratio (L_p/D_p). Despite that most monopiles are categorized in this short-rigid range, there is no research which thoroughly investigated this range to propose SR spring stiffness formulae depicting the behaviour of piles influenced by both stiffness ratio (E_s/E_p) and slenderness ratio (L_p/D_p).

This study aims to expand the applicable range of the SR spring system to the short-rigid piles and to contribute to a more accurate estimation of the first natural frequency of WTG structures with this simple analytical method. In this study, finite element (FE) models on a commercial software PLAXIS 3D are used as a reference. First of all, FE static load-displacement analyses are conducted for several monopile foundations with various slenderness ratio (L_p/D_p) embedded into a single elastic homogeneous soil stratum with different stiffness (E_s). Regarding the analytical results, a single set of SR spring stiffness formulae as a function of both the stiffness ratio (E_s/E_p) and the slenderness ratio (L_p/D_p) is proposed. The newly proposed formulae are applicable to conventional long-flexible, short-rigid and perfectly rigid piles. The first natural frequency of a structure considering the soil-pile interaction effect is theoretically estimated using the SR spring stiffness calculated from the formulae. Finally, a FE free vibration analysis is performed to validate the estimated first natural frequencies.

2. FE analysis model

2.1 Target structure

Three example WTG structures from three different wind farms with different generation capacities in the United Kingdom (Blyth: 2 MW, Barrow 3 MW and Walney1: 3.6 MW) presented in Arany et al. (2016) are investigated to make a reference model for the FE analysis. As is the case with the most typical WTG structures, the towers and the monopiles of the three

wind turbines are made of hollow steel pipes. Hereafter, for simplification of the structural model, the 'pile' is defined as the part of the monopile below the seabed whereas the 'tower' is the rest part of the structure above the seabed. The pile slenderness ratio (L_p/D_p), tower-pile length ratio (L_t/L_p), tower-pile diameter ratio (D_t/D_p), tower-pile thickness ratio (t_t/t_p) and tower-pile bending stiffness ratios (EI_t/EI_p) are firstly fixed to create the reference model, representing the commercially designed monopile and tower. The effective pile stiffness E_p is used as the parameter representing the pile stiffness. E_p is given by **Eqn. (6)** expressed by the actual bending stiffness of the pile EI_p and the area moment of inertia of a solid cylinder with the pile diameter.

$$E_p = \frac{EI_p}{\pi {D_p}^4/64} \quad (6)$$

The selected properties of the structure are listed in **Table 1**. Hereafter, the pile and tower dimensions are normalized by the monopile diameter (D_p). The Poisson's ratio of steel material and soil materials are selected to be a constant value of 0.3 because the influence of Poisson's ratio change is relatively small. However, if it is necessary, a Poisson's ratio factor proposed by Randolph (1981) can be applied to this study.

2.2 Study range

Taking the currently installed pile dimensions and its expected increase in the future into account, the probable range of the slenderness ratio (L_p/D_p) is between four and twenty. Six slenderness ratios (L_p/D_p) 4, 6, 8 ,10, 16 and 20 are selected as representative values. The stiffness ratios (E_p/E_s) are set between 0.2e3 and 960e3, that accounts for the situations to install monopiles into the softest soil (E_s = 0.075 MPa, non-consolidated soft clay) to the stiffest soil (E_s = 361 MPa, soft rock). E_p = 72.2 GPa is selected in the reference model. The

ten different stiffness ratios selected for the analyses and the corresponding soil stiffness are listed in **Table 2** with the soil numbering from one to ten.

2.3 Boundary conditions

Since the geometry and motion of a WTG structure are supposed to be symmetric against a plane parallel to the applied horizontal loading, only the half of the structure and the soil are modelled. The analysis domain is selected sufficiently large to avoid any boundary effects. The depth of the soil is at least twice as large as the pile length and the distance from the pile to the vertical side boundaries is twenty times larger than the pile diameter.

2.4 Pile modelling

Winkler approach is often used as a reference model of parametric studies or in the detailed design phase of monopiles and transition pieces (Bhattacharya 2019). In the approach, piles are modelled as a beam element without volume and the soil modelled as numbers of discs in layers with a stiffness. An advantage of using this simplified model is that the global pile deformation and internal forces (shear force and bending moment) can be easily estimated. However, the pile diameter size effect shall be accounted for in this study because the volume effect of the pile is not negligible due to the relatively small slenderness ratio of monopiles. Hence, a hybrid model (**Fig. 3**) composed of a beam element in the middle of a cylindrical solid element is employed to model a monopile taking the size effect of pile diameter into account. The bending stiffness of the pile is shared by the beam element and the solid element. The solid element is modelled to have the total weight of the monopile.

An important factor of the hybrid model is the ratio between the bending stiffness of the beam element and the solid element. The larger the bending stiffness of the beam element is to the solid element, the closer the mechanical behaviour of the hybrid model is to a single beam. However, the bending stiffness of the solid element should be large enough to ensure

the relatively stiff property of the monopile with respect to the soil at the same time so that pile-size effect is well represented. Zhang et al. (2000) made a parametric study to determine the sharing ratio between the stiffness of the beam element to the solid element and selected a ratio: nine to one for their simulation of the lateral pile loading test. The study compares the load-displacement relation and Eigen-period of a pile-ground system for several ratios and periods. Since the results with the ratio adopted by Zhang et al. (2000) look reasonable, the ratio nine to one is adopted for modelling of monopiles in this study. The Young's modulus of the solid element (7.22 GPa, 10% of the pile bending stiffness E_p) is still twenty times larger than the maximum Young's modulus of the soil (E_s) in the study range 361 MPa.

To equivalently transmit the applied loadings to the solid element on the hybrid model, a relatively rigid disc element with 50 mm of thickness is embedded at the top of the pile solid element. The tower modelled as a beam element is connected with the beam element of the pile at the seabed level.

2.5 Finite element mesh

3-node line elements are used for the tower beam element and the beam element of the hybrid pile. 6-node plate elements discretize the shell element of the soil-pile interface. The solid element of the hybrid pile and the soil are discretized by 10-node tetrahedral elements. High mesh density is selected along the pile and the soil around it to ensure the accuracy of the load-displacement analysis. The generated mesh in the analysis domain is shown in **Fig. 4**. Parameters for the soil-structure interface element are selected as the same as the surrounding soil and no slipping at the interface is accounted.

3. FE static load-displacement analysis

3.1 Overview

Sixty cases of FE static load-displacement analyses with combinations of the ten stiffness ratios and the six slenderness ratios are investigated in order to estimate the formulae of the non-dimensional stiffness (η_L, η_{LR} and η_R) as function of the stiffness ratio and slenderness ratio. Before the main analyses, the size effect of scaled piles with different diameters (1 m and 4 m) is investigated to confirm that the pile diameter in the FE analyses does not affect the non-dimensional stiffness values estimation. Hence, the scaled pile model diameter is set to the unit length 1m. A horizontal load H_1 in **Eqn. (7)** and a moment M_2 in **Eqn. (8)** are applied respectively at the seabed level and the lateral displacements u and rotations ϑ are obtained as the FE analysis results.

$$\begin{bmatrix} H_1 \\ 0 \end{bmatrix} = \begin{bmatrix} K_L & K_{LR} \\ K_{RL} & K_R \end{bmatrix} \begin{bmatrix} u_1 \\ \theta_1 \end{bmatrix} \qquad (7)$$

$$\begin{bmatrix} 0 \\ M_2 \end{bmatrix} = \begin{bmatrix} K_L & K_{LR} \\ K_{RL} & K_R \end{bmatrix} \begin{bmatrix} u_2 \\ \theta_2 \end{bmatrix} \qquad (8)$$

The four elements of the stiffness matrix are obtained solving the two matrices **Eqns. (7) and (8)**. As the coupling spring stiffness K_{LR} and K_{RL} are the same in the elastic domain, K_{LR} is used as the representative notation hereafter.

3.2 Non-dimensional spring stiffness

The SR spring stiffnesses (K_L, K_{LR} and K_R) acquired in the analysis are converted into the non-dimensional stiffnesses (η_L, η_{LR} and η_R) defined in the **Eqns. (2), (3) and (4)** which are plotted on double-logarithmic graphs. **Figure 5** shows the results of η_L as a function of stiffness ratio (E_p/E_s) with six different slenderness ratios (L_p/D_p). The plotted result lines overlap one another when the stiffness ratio (E_p/E_s) is relatively small. In this study, piles in this range are defined as long-flexible piles. Non-dimensional SR spring stiffness of the flexible piles is described by a power function of the stiffness ratio (E_p/E_s). On the other hand, there is a range where the spring stiffness converges into a constant value for each slenderness ratio

(L_p/D_p). Piles in this range are categorized as perfectly rigid piles whose non-dimensional stiffness is as a power function of the slenderness ratio. The results show that the non-dimensional spring stiffness η_L of intermediate (short-rigid) piles is as a function of both the stiffness ratio (E_p/E_s) and the slenderness ratio (L_p/D_p). The same trend is observed on the plots of η_{LR} and η_R.

3.3 Deformations and internal forces diagrams

To associate the behaviour of piles in soil with the observed SR spring stiffness trends, the deformations and internal forces observed on the whole embedded piles are also investigated, even though only the deformations at the seabed level are required for the determination of the SR spring stiffness. Pile deflection diagrams of the hybrid model when a moment is applied at the seabed level are shown in **Fig. 6** (lateral displacement diagram) and **Fig. 7** (rotation diagram) for L_p/D_p = 8, as an example. The moment is applied in a clockwise direction. Notation for the displacement to the right-hand side and for the rotation in counter-clockwise are defined positive. To plot the results for different soil stiffness, the lateral displacements are normalized to its maximum absolute value at the seabed level.

As for the lateral displacement diagram (**Fig.6**), the six cases with different soil stiffness can be globally categorized into the two groups by their deformation patterns. The piles embedded in Soil 1 and 2 seem to be categorized into flexible piles from the deflection patterns. In contrast to Soil 1 case where there is no pile toe displacement, a small pile toe displacement is observed in the pile in Soil 2. It tells that the definition of long-flexible piles in this study does not necessarily mean that the pile length is large enough to show the same behaviour of pile toe as an infinitely long pile. However, the influence of the slenderness ratio (L_p/D_p) is insignificant. As for the piles in Soils 3, 4 and 5, the deflection diagrams and the moment diagrams of these piles are very similar to that of the perfectly rigid pile in Soil 10,

257 despite that their SR spring stiffness values seem to be in the range of long-flexible or short-
258 rigid piles in **Fig. 5**.

259 As is the case with the lateral displacements, the internal forces (moment, shear force)
260 diagrams are very similar among the piles in Soils 3 ~ 10. On the other hand, the rotation
261 diagram (**Fig. 7**) of piles in Soil 1 ~ 5 (flexible to intermediate) show a remarkable difference
262 from one another. No rotational deflection is observed in Soil 10 when the pile is considered
263 as perfectly rigid.

264

265 **4. New formulae proposal**

266 **4.1 Overview**

267 The next step is the proposal of a new set of formulae for the SR spring stiffness estimation
268 by means of curve fittings on the double-logarithmic graphs with the stiffness ratio on the x-
269 axis and the non-dimensional stiffness η_L, η_{LR} and η_R on the y-axis. The common-logarithm
270 of the non-dimensional stiffness: $\log_{10}(\eta_L)$, $\log_{10}(-\eta_{LR})$, $\log_{10}(\eta_R)$ linearly increases as a
271 function of common-logarithm of the stiffness ratio: $X = \log_{10}(E_p/E_s)$ for flexible piles with
272 relatively small stiffness ratios (E_p/E_s) and it reaches a constant value for rigid piles with
273 relatively large stiffness ratios. The non-dimensional stiffness in the intermediate (short-rigid
274 pile) range depicts non-linear curves connecting the linear function and the constant function.

275 **4.2 Sigmoid**

276 To fit these "S-shaped curves" $f_i(X)$, the sigmoid curve function may well represent the
277 stiffness features. The most generalized sigmoid function is the Richards curve **Eqn. (9)** named
278 after F.J. Richard, who developed the simple logistic growth curve proposed by Pierre Verhulst
279 as a population growth model (Richards 1959; Bacaër 2011).

$$f_i(X) = L_{-\infty} + \frac{L_{+\infty} - L_{-\infty}}{\left(1 + Ae^{-B(X - x_0)}\right)^{1/C}} \quad (9)$$

The Richards curve has six parameters: $L_{+\infty}$, $L_{-\infty}$, x_0 , B, A and C. In this study, four parameters ($L_{+\infty}$, $L_{-\infty}$, x_0 and B) out of the six are defined as a function of the slenderness ratio. For the remaining two (A, C), a constant value $A = 1$ and $C = 100$ are selected, and eliminated from the parameter study.

4.3 Parameters

The parameters are determined by trial and error using the non-linear least square method on the Matlab curve fitting toolbox until most of the errors between the FE load-displacement results and the sigmoid function are within a relatively narrow band (± 3.5 % for K_L, ± 4 % for K_{LR} and ± 7 % for K_R). Regarding K_{LR} and K_R, the accuracy of short-rigid piles is prioritized than that of slender piles because the relatively rigid range is the most important range for monopile designers. Errors up to 7% and 14 % are observed in case of K_{LR} (L_p/D_p: 20) and K_R (L_p/D_p: 16 and 20), respectively. Each of the four parameters has a special characteristic on the data curves. These are determined one after another in the following order.

1. $L_{+\infty}\left(L_p/D_p\right)$: Upper asymptote
2. $x_0\left(L_p/D_p\right)$: Inflection point
3. $L_{-\infty}\left(L_p/D_p\right)$: Lower asymptote
4. $B\left(L_p/D_p\right)$: Sharpness of the curve

4.4 Proposal and evaluation

Twelve closed-form equations to determine the four parameters ($L_{+\infty}$, $L_{-\infty}$, x_0 and B) for each spring stiffness ratio (η_L, $-\eta_{LR}$ and η_R) are proposed and listed in **Table 3**. The proposed sigmoid curves (solid lines), the SR spring stiffness values estimated from the FE analysis, the formulae of Gazetas (1984) (dashed lines) for flexible piles and the formulae of Higgins et al.

(2013) (dotted lines) for rigid piles are plotted on the same graphs (**Figs. 8 ~ 10**) for comparison. The sigmoid curves match very well with the formulae of Gazetas (1984) in the flexible pile range and with the formulae of Higgins et al. (2013) in the perfectly rigid pile range.

5. First natural frequency estimation

5.1 Overview

According to the previous studies such as Zaaijer (2006) and Arany (2016), the effect of the soil-pile interaction is often too large to be ignored in the natural frequency estimation of WTG structures. The actual natural frequencies f_n accounting for the foundation stiffness are lower than the fixed-base frequencies f_{FB} assuming cantilever beam with a rigid boundary condition at seabed level. Free vibration study in an analytical method is performed on a simplified tower structure supported by the SR spring system, and the first natural frequency of the structure f_1 is estimated based on the Euler-Bernoulli beam theory applicable to flexible structures. Arany et al. (2015) report that the Euler-Bernoulli beam model is accurate enough to calculate the first natural frequency of a WTG tower because the effect of shear deformation is not significant.

5.2 Equation of motion

The first natural frequency of the structure is estimated by a free vibration on an Euler-Bernoulli beam supported by the SR springs. The equation of motion for an Euler-Bernoulli beam is written as the following **Eqn. (10)**.

$$\mathbb{M}\ddot{\mathbb{u}} + \mathbb{K}\mathbb{u} = \mathbb{O} \quad (10)$$

As the tower has a distributed mass along the structure, calculation of this matrix equation is computationally expensive. For further simplification of the model to reduce the number of the degree of freedom, an effective mass (M_{eff}) at the top of the tower is introduced. The

effective mass is defined by equating the kinematic energy of the cantilever beam with the distributed mass and that of a cantilever beam with an effective mass (M_{eff}) at the top of the beam. Following the calculation documented in Gürgöze (2005), M_{eff} is expressed as a function of the mass of the tower m_t and the mass of the nacelle m_{RNA} as presented in **Eqn. (11)**.

$$M_{eff} = \frac{33}{140} m_t + m_{RNA} \qquad (11)$$

This simplified model has three degrees of freedom. The first nodal displacement u is the relative displacement between the tower top and the seabed in the horizontal direction. The second nodal displacement u_b and the third nodal rotation θ_b is at the seabed in the lateral direction and the rotational direction, respectively. The absolute nodal displacement vector in the equation of motion (**Eqn. (10)**) is written in **Eqn. (12)**. This method is used by Chowdhury (2016).

$$\mathbb{u} = \begin{bmatrix} u + u_b + \theta_b L_t \\ u_b \\ \theta_b \end{bmatrix} \qquad (12)$$

5.3 First natural frequency

Supposing that the nodal displacement vector has a harmonic solution, the equation of motion (10) is transformed into **Eqn. (13)**.

$$(\mathbb{K} - \omega^2 \mathbb{M})\mathbb{u} = \mathbb{O} \qquad (13)$$

The mass matrix **Eqn. (14)** is defined only with the effective mass when the mass effect of the pile is very small.

$$\mathbb{M} = \begin{bmatrix} M_{eff} & & \\ & 0 & \\ & & 0 \end{bmatrix} \qquad (14)$$

The stiffness matrix **Eqn. (15)** can be obtained by applying either the force method or the displacement method to the system.

$$\mathbb{K} = \begin{bmatrix} K_t & -K_t & -K_t L_t \\ -K_t & K_t + K_L & K_t L_t + K_{LR} \\ -K_t L_t & K_t L_t + K_{RL} & K_t {L_t}^2 + K_R \end{bmatrix} \quad (15)$$

The stiffness matrix elements are described with the combinations of tower lateral stiffness for the first mode K_t: **Eqn. (16)**, the tower height L_t and the SR spring stiffness (K_L, K_{LR} and K_R).

$$K_t = \frac{3EI_t}{{L_t}^3} \quad (16)$$

To obtain a unique solution from Eq. (13), the determinant of the matrix $(\mathbb{K} - \omega^2 \mathbb{M})$ should be zero. Introducing the following non-dimensional stiffness normalized by the tower stiffness and the tower height (ζ_L^*: **Eqn. (17)**, ζ_{LR}^*: **Eqn. (18)**, ζ_R^*: **Eqn. (19)**) and the fixed-base angular velocity of the first mode ($\omega_{FB,1}$: **Eqn. (20)**), the determinant of the matrix $(\mathbb{K} - \omega^2 \mathbb{M})$ is calculated.

$$\zeta_L^* = \frac{K_L}{K_t} \quad (17)$$

$$\zeta_{LR}^* = \frac{K_{LR}}{K_t L_t} \quad (18)$$

$$\zeta_R^* = \frac{K_R}{K_t {L_t}^2} \quad (19)$$

$$\omega_{FB,1} = \sqrt{\frac{K_t}{M_{eff}}} \quad (20)$$

The ratio of the natural frequency of the structure to the fixed-base frequency for the first mode ($f_1/f_{FB,1}$) is estimated in the following **Eqn. (21)** with the soil-pile-tower interaction factor χ: **Eqn. (22)**.

$$\frac{f_1}{f_{FB,1}} = \frac{\omega_1}{\omega_{FB,1}} = \sqrt{1 - \frac{1}{1+\chi}} \quad (21)$$

$$\chi = \frac{\zeta_L^* \zeta_R^* - {\zeta_{LR}^*}^2}{\zeta_L^* - 2\zeta_{LR}^* + \zeta_R^*} = \frac{1}{K_t} \cdot \frac{K_L \cdot K_R - {K_{LR}}^2}{K_L {L_t}^2 - 2K_{LR} L_t + K_R} \quad (22)$$

The factor χ is the same for the proportionally enlarged structure models because it only depends on the non-dimensional spring stiffness normalized by the tower stiffness.

6. FE free vibration analysis

6.1 Overview

As the factor χ does not change, even if the structure size proportionally enlarged, the pile and tower model with D_p = 1 m is used in the FE free vibration analysis to validate the natural frequencies estimated in the theoretical calculation. In this study, m_{RNA} is defined as zero and m_t is calculated from the density of steel and the volume of the tower. A Newmark β value of one-fourth is selected to ensure the calculation stability and at least five structural vibration waves are investigated after releasing a horizontal loading at the tower head. Even though the material damping ratios of the soil, pile and tower are set to zero, an unknown damping ratio ξ, which is defined by the angular velocity of the first mode ω_1 and the angular velocity with damping ω_D (**Eqn. (23)**), is observed in the results.

$$\omega_D = \omega_1\sqrt{1-\xi^2} \quad (23)$$

6.2 Natural frequency validation

Eliminating the effect of the damping, the first natural frequencies determined by the FE free vibration analysis (open circles) are compared with the theoretical estimation (solid lines) in **Fig. 11**. Even though the "Inverse-S shaped" curves are well depicted within the theoretical model using the proposed sigmoid functions, the frequency values are overestimated in the cases with small slenderness ratios L_p/D_p= 4 and 8. This kind of overestimation of the natural frequency with the SR spring system is also reported in previous studies, for example by Okada et al. (2007).

To investigate a cause of the natural frequency overestimation, a parameter study is conducted. From a free vibration analysis for an extreme case with the pile and soil mass, which is nearly zero, it is confirmed that the effect of the embedded pile mass is negligible in the first natural frequency estimation and not a reason of the overestimation. The overestimation of the natural frequency cannot be explained by the effective mass M_{eff} nor the tower length L_t because the first natural frequency estimation is very accurate in cases with the relatively stiff soil materials (E_p/E_s= 0.2e3).

Hence, the only reason which can explain the natural frequency overestimation is the parameters of the SR spring stiffness. As seen in **Fig. 11**, the SR spring method result curve matches perfectly if a dynamic pile effective stiffness $E_{p\_dynamic}$, which is 1.75 times smaller than static pile effective stiffness E_p, is selected to determine the SR spring stiffness in the case of L_p/D_p = 4. On the other hand, 2.25 times smaller E_p should be selected as $E_{p\_dynamic}$ in case of L_p/D_p = 8. The dynamic stiffness of the pile to be used in the SR dynamic analysis differs from the static pile stiffness. The statement is supported by the research of Novak et al. (1977). According to his research group, the modification of pile stiffness and consideration of damping generation are required in dynamic models due to the energy radiation and dissipation caused by the soil-pile interaction. The modification is proposed to be a non-linear change with respect to the soil and pile properties. It is verified that the first natural frequency can be estimated with a high accuracy taking the dynamic pile stiffness effect into account. However, further study is required to obtain the ratio between the static pile effective stiffness E_p and the dynamic pile effective stiffness $E_{p\_dynamic}$.

7. Contribution of new formulae

7.1 Overview

The accuracy of the newly proposed formulae is evaluated and justified in this section. The SR spring stiffness, deformations at the seabed level and the first natural frequencies are estimated with the bilinear curves (dashed lines in **Fig. 12**) with an abrupt transition from long-flexible to perfectly rigid behaviour and the newly proposed sigmoid curves (solid lines in **Fig. 12**). In the following subsections, the results of the two different formulae for three representative slenderness ratios (L_p/D_p = 4, 8, 20) are compared. At the end of this section, how to use the new set of formulae in practice is presented.

7.2 SR spring stiffness

The bilinear curves are defined by extrapolating the long-flexible pile linear function and the rigid pile constant function in the double-logarithmic graphs. The limitation of the previously proposed equations is that the behaviour of short-rigid piles is not described in the equations. As seen in **Fig. 12**, the SR spring stiffness is overestimated in the short-rigid pile cases compared to the sigmoid formulae. The errors due to the negligence of the short-rigid pile effects are defined by the following error function (**Eqn. (24)**).

$$Error = \left(\frac{X(\text{bilinear})}{X(\text{sigmoid})} - 1\right) \times 100\ [\%] \quad (24)$$

X is substituted by η, u, θ or f_1 to calculate the corresponding errors. The maximum errors in the SR spring stiffness estimations among the three slenderness ratios are 16.7% (K_L), 28.9% (K_{LR}) and 52.6% (K_R) and are located at the intersections of the bilinear curves for the slenderness ratio $L_p/D_p = 4$. The smaller the slenderness ratio is, the larger errors are observed. This means that contribution of the new formulae is large for short-rigid piles such as monopiles. These SR estimation errors cause errors in the estimation of the deformations and the first natural frequency.

7.3 Deformations at seabed level

The lateral displacement and the rotation intensity is highly depending on the applied static loading at the seabed level. A total (static and dynamic) lateral loading-moment combination under the yearly mean wind speed 20 m/s is estimated to be (*H*, *M*) = (1.79 MN, 121.5 MNm) according to Arany et al. (2014). These loadings are selected as the largest service state load in this study. Due to the overestimation of the SR spring stiffness, the lateral displacement and the rotation at the seabed level tend to be underestimated in the simple bilinear estimation as seen in **Fig. 13**. The error values hit 41.3% (4.2e-2 [m]: sigmoid and 2.5e-2 [m]: bilinear) for the lateral displacement and 46.9% (4.9e-3 [rad]: sigmoid and 2.6e-3 [rad]: bilinear) for the rotation at E_p/E_s = 2.5e3 in the case of L_p/D_p = 4.

According to DNVGL-ST-0126 (2018), the rotational allowance due to the excitation loadings is 0.25°, which is equal to 4.4e-3 [rad]. Selecting L_p/D_p = 4 as an example, the effective pile stiffness E_p is supposed to be 1.5 times overestimated by the bilinear function (E_p/E_s = 3.3e3) than the sigmoid function (E_p/E_s = 2.2e3) when the soil stiffness is the same. The difference might be significantl in the design phase. The newly proposed sigmoid formulae should be used instead of the bilinear formulae to select sufficient pile dimensions to fulfil the design requirements.

7.4 First natural frequency

As demonstrated in Section 6, the ratio of the first natural frequency of the structure to the fixed-base frequency ($f_1/f_{FB,1}$) is determined by the soil-pile-tower factor χ depending on the non-dimensional spring stiffness normalized by the tower stiffness. The ratio calculated by the sigmoid formulae and the bilinear formulae is compared in **Fig. 14**. The maximum errors of the f_1/f_{FB} are 7.3% (L_p/D_p = 4, E_p/E_s = 2.5e3), 10.3% (L_p/D_p= 8, E_p/E_s= 3.2e4) and 5.0% (L_p/D_p= 20, E_p/E_s = 9.3e4).

When the structure fixed-base frequency $f_{FB,1}$ is 0.2 ~ 0.8 Hz, the 10% error of the first natural frequency f_1 can be equal to 0.01 ~ 0.05 Hz. This error range might have a significant influence in some projects in which the first natural frequency of structures should fall within a very small range between rotor frequency: 1P (0.08 ~ 0.22 Hz) and the blades passing frequency: 3P (0.25 ~ 0.65 Hz) (Data source: Arany et al. 2016). In the case of a turbine generation with a capacity of 8 MW or larger, the frequency band between 1P and 3P is only 0.03 Hz (0.22 ~ 0.25 Hz).

7.5 How to use the formulae

This subsection aims to explain how the newly developed formulae can be practically used. If the sequence is once understood and traced in a simple calculation tool such as Microsoft Excel, it will take only a few minutes to calculate (i) SR spring values (K_L, K_{LR} and K_R), (ii) displacement and rotation at seabed level and (iii) first natural frequency of the structure.

First of all, the effective pile stiffness E_p, soil stiffness E_s, embedded pile length L_p and pile diameter D_p shall be defined. Secondly, four parameters ($L_{+\infty}$, $L_{-\infty}$, x_0 and B) shall be calculated with **Table 3** by substituting the parameter L_p/D_p with an actual value. The non-dimensional stiffness (η_L, $-\eta_{LR}$ and η_R) can be obtained by substituting the parameter E_p/E_s and the four parameters ($L_{+\infty}$, $L_{-\infty}$, x_0 and B) of **Eqn. (9)**. The remaining two parameters (A and C) excluded from the parameter study are one and a hundred, respectively. Or alternatively, η_L, $-\eta_{LR}$ and η_R can be roughly estimated using **Fig. 8**, **Fig. 9** and **Fig. 10**. Note that $\eta_{LR}$is negative. K_L, K_{LR} and K_R shall be calculated using **Eqn. (2), (3) and (5)**.

Eqn. (1) enables to obtain the lateral displacement and rotation at the seabed level. As for the first natural frequency of the structure, please follow the steps written in Section 5.2 and 5.3.

The following properties of the tower: mass of tower m_t, mass of nacelle m_{RNA}, diameter of tower D_t, thickness of tower t_t and height of tower L_t are additionally required to estimate the first natural frequency of the structure. With the parameters, the effective mass M_{eff} and K_t shall be defined with the **Eqn. (11)** and **Eqn. (16)**. Assuming that the tower is perfectly fixed to the ground, the fixed-base angular velocity ($\omega_{FB,1}$) or fixed-base frequency ($f_{FB,1}$) is obtained as a function of M_{eff} and K_t. The stiffness ratios between the Sway-Rocking (SR) spring stiffness and the tower stiffness (ζ_L^*, ζ_{LR}^*, ζ_R^*) can be defined by **Eqns. (17), (18) and (19)**. The ratio between the natural frequency of the structure and the fixed-base frequency for the first mode ($f_1/f_{FB,1}$) can be simply determined with the soil-pile-tower interaction factor χ calculated by **Eqn. (22)**.

8. Conclusions

A new set of formulae of the Sway-Rocking (SR) extend the application of the SR spring system, which was limited to long-flexible and perfectly rigid foundations, to 'short-rigid' piles. The new SR spring stiffness formulae is a function of the stiffness ratio (E_p/E_s) and slenderness ratio (L_p/D_p). The study range of the soil and pile properties are chosen such that it simulates currently used offshore wind monopile foundations. The methodology to estimate the displacement at seabed level and the first frequency with the SR spring system is also demonstrated in this paper.

Improvement of the SR spring stiffness accuracy is maximum of 16.7% (K_L), 28.9% (K_{LR}) and 52.6% (K_R) with the slenderness ratio $L_p/D_p = 4$. Along with the improvement of the SR spring stiffness estimation, accuracy of the deformation and natural frequency are also improved. In an example case of a pile with a stiffness ratio $E_p/E_s = 2.5\mathrm{e}3$, slenderness ratio $L_p/D_p = 4$, horizontal loading $H = 1.79$ MN and moment $M = 121.5$ MNm, the expected

deformation differs maximum by 41.3 % for the lateral displacement and by 46.9% for the rotation. The ratio of the first natural frequency to the fixed-base frequency $f_1/f_{FB,1}$ can be estimated 10.3 % more accurately with the new formulae than the existing bilinear formulae ($E_p/E_s = 3.2\text{e}4$ and $L_p/D_p = 8$). The first natural frequency considering the soil-pile interaction can be well estimated by this method. However, the accuracy of the estimation may be improved by introducing the "dynamic" pile effective stiffness $E_{p\_dynamic}$ instead of the "static" pile stiffness E_p.

Acknowledgements

The first author studied at ENPC to obtain the engineering degree besides the master degree of Tokyo Tech, financially supported by BGF and Tobitate. This research topic has been selected by the author who was inspired by her ENPC supervisors Jean-Michel Pereirra and Aphrodite Michael as well as her colleagues during an internship at Mott MacDonald.

References

Arany L, Bhattacharya S, Macdonald J, Hogan SJ (2014) Simplified critical mudline bending moment spectra of offshore wind turbine support structures. Wind Energy, Vol. 18 (2015), 2171-2197 https://doi.org/10.1002/we.1812

Arnay L, Bhattacharya S, Adhiakari S, Hogan SJ, Macdonald J (2015) An analytical model to predict the natural frequency of offshore wind turbines on three-spring flexible foundations using two different beam models. Soil Dynamics and Earthquake Engineering, Vol. 74, 40-45 https://doi.org/10.1016/j.soildyn.2015.03.007

Arany L, Bhattacharya S, Macdonald J, Hogan SJ (2016) Closed form solution of Eigen frequency of monopile supported offshore wind turbines in deeper waters

incorporating stiffness of substructure and SSI. Soil DynamicsandEarthquakeEngineering, Vol. 83, 18–32 https://doi.org/10.1016/j.soildyn.2015.12.011

Bacaër N (2011) Verhulst and the logistic equation (1838). In: A Short History of Mathematical Population Dynamics. Springer-Verlag London, London, pp.35-39 https://doi.org/10.1007/978-0-85729-115-8_6

Bhatacharya S (2019) Design of foundation for foundations for offshore wind turbines. New Jersey, USA: Wiley

Byrne BW et al. (2020) Editorial: geotechnical design for offshore wind turbines monopiles, Geotéchnique, Vol. 70, No. 11, 943-944 https://doi.org/10.1680/jgeot.2020.70.11.943

Carter BJP, Kulhawy FH (1992) Analysis of laterally loaded shaft in rock. Journal of Geotechnical Engineering, Vol. 118, No. 6, 839-855 https://doi.org/10.1061/(ASCE)0733-9410(1992)118:6(839)

Chowdhury I, Tarafdar R, Ghosh A, Dasgupta SP (2016) Dynamic response of cylindrical structure considering coupled soil-structure interaction under seismic loading. Bull Earthquake Engineering, Vol.14, 2329-2360 https://doi.org/10.1007/s10518-016-9909-4

DNV (2002) Guidelines for Deign of Wind Turbines. London, UK: DNV/Risø

DNVGL-RP-C212 (2017) Recommended practice. DNVGL-RP-C212 Offshore soil mechanics and geotechnical engineering. DNV GL AS, Edition August 2017

DNVGL-ST-0126 (2018) Standard. DNVGL-ST-0126 Support structures for wind turbines. DNV GL AS, Edition July 2018

554 EN1998-5 (2004) Eurocode 8: Design of structures for earthquake resistance – Part 5:
555 Foundations, retaining structures and geotechnical aspects. The European Union, 36
556 (Annex C)
557 Fleming WGK, Weltman AJ, Randolph MF et al. (1992) Pilling Engineering. Glasgow, UK:
558 Blackie
559 Gazetas G (1984) Seismic response of end-bearing single piles. International Journal of Soil
560 Dynamics and Earthquake Engineering, 1984, Vol. 3, No. 2, 82-93
561 https://doi.org/10.1016/0261-7277(84)90003-2
562 Gürgöze M (2005) On the representation of a cantilevered beam carrying a tip mass by an
563 equivalent spring-mass system. Journal of Sound and Vibration, Vol.282, 538-542
564 https://doi.org/10.1016/j.jsv.2004.04.006
565 Higgins W, Vasquez C, Basu D, Griffiths DVG (2013) Elastic solutions for laterally loaded piles.
566 Journal of geotechnical and geoenvironmental engineering, ASCE, Vol. 139, No. 7,
567 1096-1103 https://doi.org/10.1061/(ASCE)GT.1943-5606.0000828
568 IRENA (2019) A Global Energy Transformation paper -FUTURE OF WIND.
569 https://www.irena.org/-
570 /media/Files/IRENA/Agency/Publication/2019/Oct/IRENA_Future_of_wind_2019.pdf
571 . Accessed 15 November 2020
572 Novak M, Nogami T (1977) Soil-pile interaction in horizontal vibration. Earthquake
573 Engineering and Structural Dynamics, Vol.5, 263-281
574 https://doi.org/10.1002/eqe.4290050305
575 Okada T, Unjoh S (2007) Analytical study on the damping factor of bridge foundations. JSCE
576 journal of Earthquake Engineering, Vol. 29, 381-388
577 https://doi.org/10.11532/proee2005a.29.381

578 Randolph MF (1981) The response of flexible piles to lateral loading. Geotéchnique, Vol. 31,
579 No. 2, 247-259 https://doi.org/10.1680/geot.1981.31.2.247
580 Richards FJ (1959) A flexible growth function for empirical use. Journal of Experimental
581 Botany, Vol. 10, No. 2, 290 –301 https://www.jstor.org/stable/23686557
582 Shadlou M, Bhattacharya S (2016) Dynamic stiffness of monopiles supporting offshore wind
583 turbine generators. Soil Dynamics and Earthquake Engineering , Vol. 88, 15-32
584 https://doi.org/10.1016/j.soildyn.2016.04.002
585 Wind-Europe (2017) The European offshore wind industry Key trends and statistics 2016.
586 https://windeurope.org/wp-content/uploads/files/about-
587 wind/statistics/WindEurope-Annual-Offshore-Statistics-2016.pdf. Accessed 12 April
588 2020
589 Zaaijer MB (2006) Foundation modelling to assess dynamic behaviour of offshore wind
590 turbines. Applied Ocean Research, Vol.28, 45-57
591 https://doi.org/10.1016/j.apor.2006.03.004
592 Zhang F, Kimura M, Nakai T, Hoshikawa T (2000) Mechanical behavior of pile foundations
593 subjected to cyclic lateral loading up to the ultimate state. Soils and foundations, Vol.
594 40, No. 5, 1-17 https://doi.org/10.3208/sandf.40.5_1
595 4C Offshore (2018), Offshore wind farms database.
596 https://www.4coffshore.com/windfarms/. Accessed 12 April 2020
597

598 **Nomenclature**

Nomenclature

H	Lateral force at the seabed [N]	E_s	Young's modulus of soil [Pa]	m_t	Total mass of tower [kg]
M	Moment at the seabed [Nm]	E_p	Effective pile stiffness [Pa]	m_{RNA}	Mass of RNA [kg]
u	Lateral displacement [m]	ν	Poisson's ratio [-]	ω_1	Angular velocity (1st mode) [rad/s]
θ	Rotational displacement [rad]	L_p	Embedded length of pile [m]	ω_{FB}	Fixed-base angular velocity [rad/s]
K_L	Lateral spring stiffness [N/m]	D_p	Diameter of pile [m]	f_1	Natural frequency (1st mode) [Hz]
K_{LR}	Coupling spring 1 stiffness [N/rad]	t_p	Wall thickness of pile [m]	f_{FB}	Fixed-base natural frequency [Hz]
K_{RL}	Coupling spring 2 stiffness [Nm/m]	EI_p	Bending stiffness of pile [Nm^2]	ζ_L	K_L normalized by K_t and L_t [-]
K_R	Rotational spring stiffness [Nm/rad]	L_t	Tower height [m]	ζ_{LR}	K_{LR} normalized by K_t and L_t [-]
η_L	K_L normalized by E_s and D_p [-]	D_t	Diameter of tower [m]	ζ_R	K_R normalized by K_t and L_t [-]
η_{LR}	K_{LR} normalized by E_s and D_p [-]	t_t	Wall thickness of tower [m]	χ	Soil-pile-tower interaction factor [-]
η_{RL}	K_{RL} normalized by E_s and D_p [-]	EI_t	Bending stiffness of tower [Nm^2]	ω_D	Angular velocity with damping [rad/s]
η_R	K_R normalized by E_s and D_p [-]	K_t	Tower stiffness in lateral way [N/m]	ξ	Damping ratio [-]
		M_{eff}	Effevtive mass at the top of tower [kg]	$E_{p\_dynamic}$	Dynamic pile effective stiffness [Pa]

599

Figures

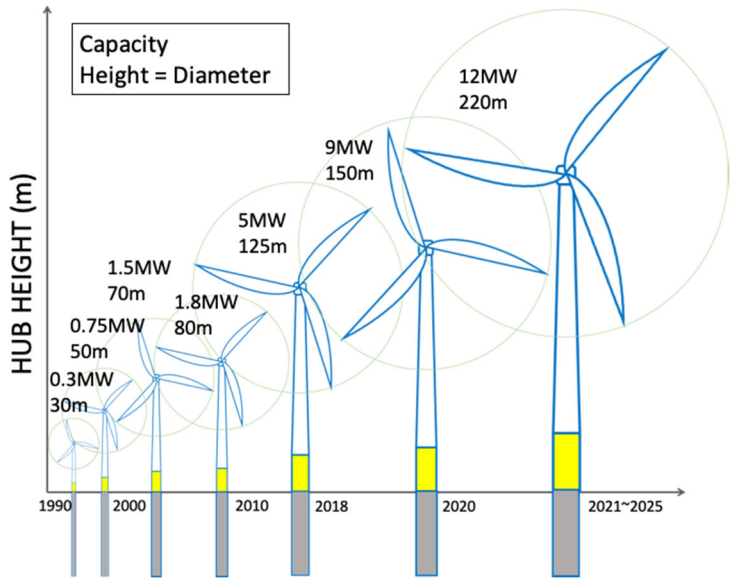

Fig. 1. Growth in size of commercial turbines

(Data source: Wind-Europe 2017; 4C Offshore 2018; and IRENA 2019)

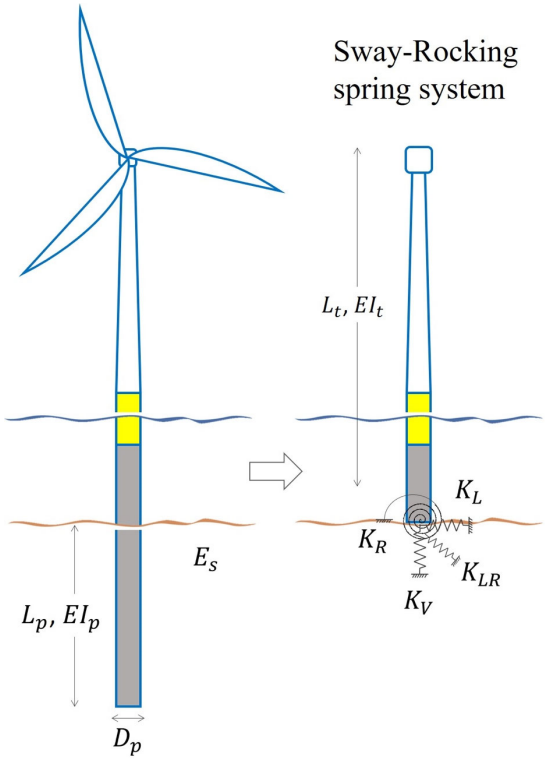

Fig. 2. Sway-Rocking spring system

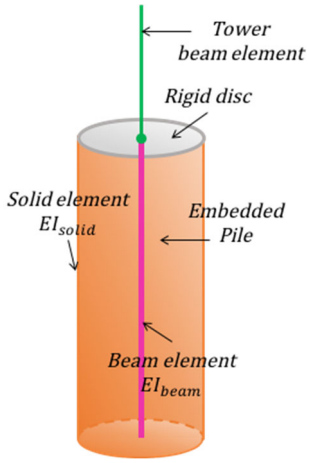

608

609 Fig. 3. Hybrid pile model

610

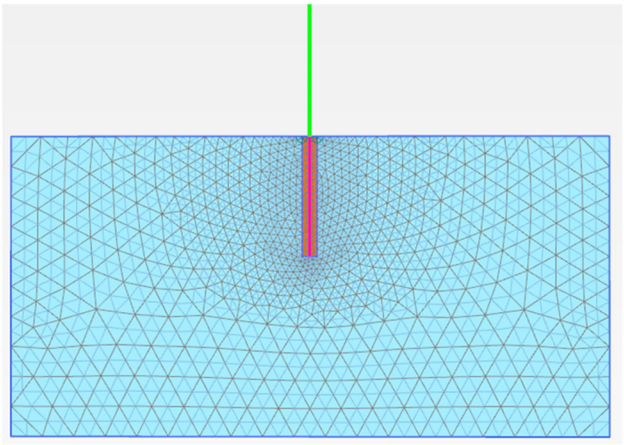

611

612 Fig. 4. Generated mesh in the analysis domain ($L_p/D_p = 8$)

613

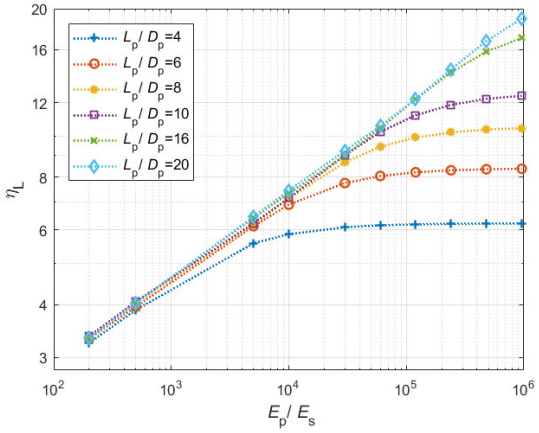

614

615 Fig. 5. Non-dimensional stiffness (η_L), FE static load-displacement result

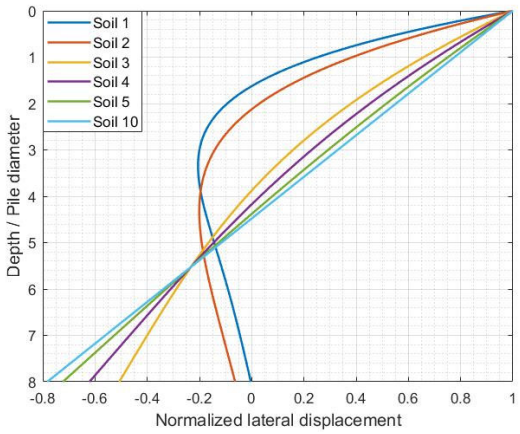

Fig. 6. Lateral displacement diagram (M) where $L_p/D_p = 8$

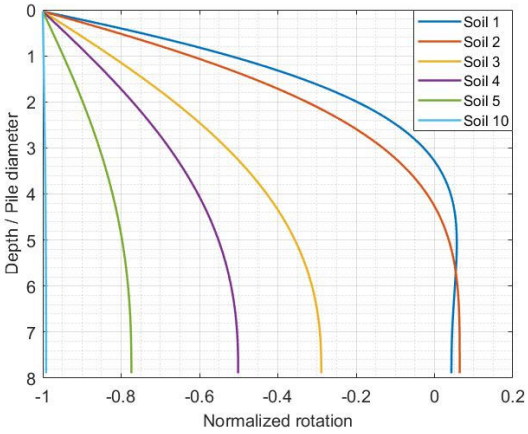

Fig. 7. Rotation diagram (M) where $L_p/D_p = 8$

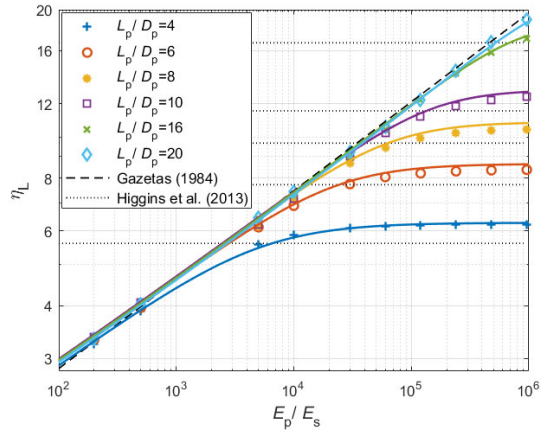

623

624 Fig. 8. Non-dimensional stiffness (η_L), FE static load-displacement analysis vs. Sigmoid

625 curves and curves appear in literature

626

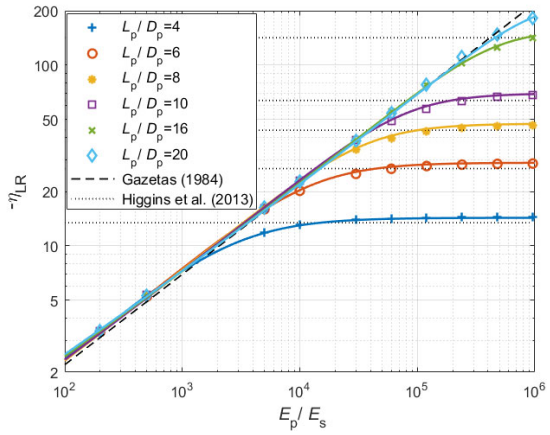

627

628 Fig. 9. Non-dimensional stiffness ($-\eta_{LR}$), FE static load-displacement analysis vs. Sigmoid

629 curves and curves appear in literature

630

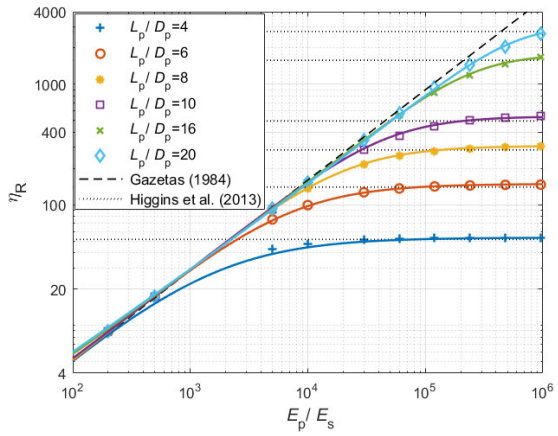

631

632 Fig. 10. Non-dimensional stiffness (η_R), FE static load-displacement analysis vs. Sigmoid

633 curves and curves appear in literature

634

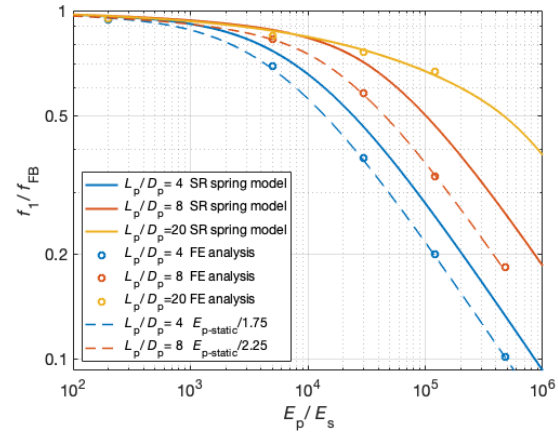

635

636 Fig. 11. Comparison of f_1/f_{FB}, Theoretical estimation vs. FE free vibration analysis

637

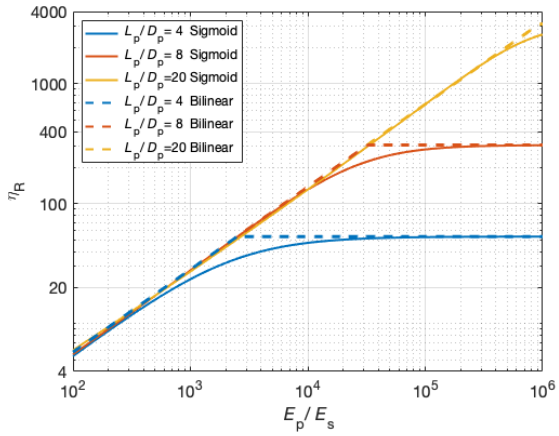

638

639 Fig. 12. Non-dimensional SR spring stiffness (η_L), Sigmoid curves vs. Bilinear curves

640

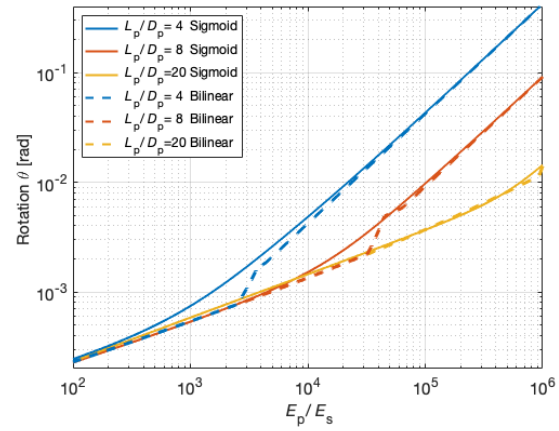

641

642 Fig. 13. Estimation of rotation, Sigmoid curves vs. Bilinear curves

643

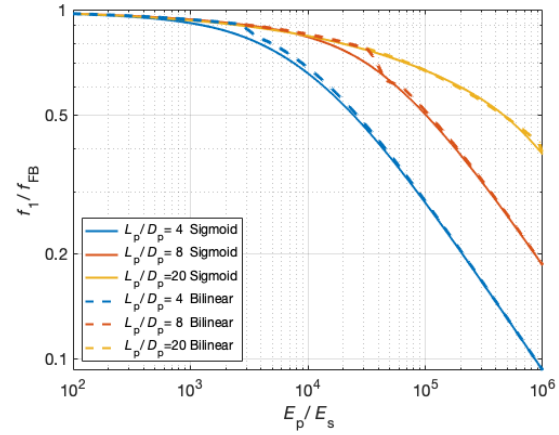

644

645 Fig. 14. Estimation of the first natural frequency, Sigmoid curves vs. Bilinear curves

Tables

Table 1. Fixed properties of the tower and monopile of the reference model

Tower Diameter	Tower wall thickness	Tower height	Pile Diameter	Pile wall thickness	Steel unit weight	Young's modulus of steel	Effective Young's modulus of piles
D_t	t_t	L_t	D_p	t_p	γ_{steel}	E_{steel}	E_p
0.75 m	0.03 m	20 m	1.00 m	0.05 m	78 kN/m^3	210 GPa	72.2 GPa

Table 2. Ten selected stiffness ratios and corresponding soil stiffness

	Soil 1	Soil 2	Soil 3	Soil 4	Soil 5	Soil 6	Soil 7	Soil 8	Soil 9	Soil 10
E_p/E_s [-]	0.2e3	0.5e3	5.0e3	10e3	30e3	60e3	120e3	240e3	480e3	960e3
E_s [MPa]	361	144	14.4	7.22	2.40	1.20	0.60	0.30	0.15	0.075

Table 3. List of closed-form equations for the four parameters

Parameter $L_{+\infty}$	$L_{+\infty}(\eta_L) = \log_{10}\left(2.1 \cdot \left(L_p/D_p\right)^{0.79}\right)$
	$L_{+\infty}(-\eta_{LR}) = \log_{10}\left(1.3 \cdot \left(L_p/D_p\right)^{1.73}\right)$
	$L_{+\infty}(\eta_R) = \log_{10}\left(1.6 \cdot \left(L_p/D_p\right)^{2.53}\right)$
Parameter $L_{-\infty}$	$L_{-\infty}(\eta_L) = -13 \cdot \left(L_p/D_p\right)^{-0.35}$
	$L_{-\infty}(-\eta_{LR}) = -32 \cdot \left(L_p/D_p\right)^{-0.35}$
	$L_{-\infty}(\eta_R) = -89 \cdot \left(L_p/D_p\right)^{-0.55}$
Parameter x_0	$x_0(\eta_L) = 3.68 \cdot \log_{10}\left(L_p/D_p\right) + 1.47$
	$x_0(-\eta_{LR}) = 3.68 \cdot \log_{10}\left(L_p/D_p\right) + 1.22$
	$x_0(\eta_R) = 3.68 \cdot \log_{10}\left(L_p/D_p\right) + 0.97$
Parameter B	$B(\eta_L) = 1.5 \cdot \left(L_p/D_p\right)^{0.31}$
	$B(-\eta_{LR}) = 1.9 \cdot \left(L_p/D_p\right)^{0.24}$
	$B(\eta_R) = 1.1 \cdot \left(L_p/D_p\right)^{0.41}$